Supplementary materials (SM1, SM2, SM3, SM4) of manuscript

"Experimental and numerical investigation of the transition from non sooting to sooting premixed n-butane flames, encompassing the nucleation flame conditions"

from C. Betrancourt, D. Aubagnac-Karkar, X. Mercier, A. El-Bakali, P. Desgroux

Combustion and Flame

SM1: Input temperature profiles used for modelling

As mentioned in section 2.2, the sharp temperature gradient and the associated induced beam steering prevented to measure the temperature profile accurately at low HAB. In order to circumvent this inconvenient, we used an approach close to that used in Bejaoui et al. [1] combining the temperatures calculated by solving the enthalpy equation with the experimental ones measured in the burnt gases, at the burner surface and at the stabilization plate location, in order to rebuilt the temperature profiles in each flame.

One dimensional impinging jet equations are solved using the measured inlet conditions for species and mass flow. The enthalpy transport equation is solved to get the temperature taking into account H_2O CO, CH_4 and CO_2 radiation with the optically thin radiation model proposed by Liu and Rogg [2] available in Cantera and imposing inlet and surface temperatures. Soot radiation is neglected in this work due to its very low concentration with a maximum of 9.8 ppb in Flame1.95. Inlet temperature are set through testing so that the predicted temperatures meet the first (i.e. closest of the burner) measured ones and the stabilization plate temperatures used are the one measured experimentally. This lead to inlet temperatures of 850K, 900K and 450K for flames at ϕ = 1.6, ϕ = 1.75, ϕ = 1.95 respectively. Figure 1 shows the experimental temperature profiles (symbols) and those obtained from the simulations (lines). The differences between the measured and predicted temperatures for the three mechanisms are acceptable given the uncertainties in the temperature measurements. The experimental temperatures at 16 mm correspond to the plate temperature.

Though imperfect, we believe that this approach allows minimizing the human artefacts in the final selection of the temperature profiles which serve as input in the modelling. For each mechanism, the temperature profiles have been computed with and without soot model, with less than 10K difference between both at every point of every case. Moreover, the difference between the temperature profile predicted by POLIMI and the two other mechanisms has been checked to be non-influential of the results presented in the manuscript.

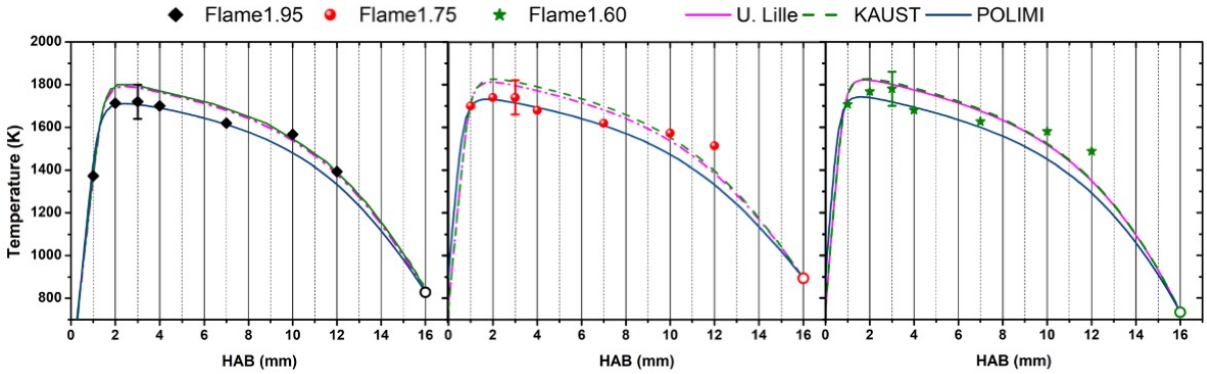

Figure 1. Comparison of measured temperature profiles (symbols) and those modelled (lines) of atmospheric n-butane/O_2/N_2 flame at ϕ = 1.60, ϕ = 1.75 and ϕ = 1.95.

[1] S. Bejaoui, S. Batut, E. Therssen, N. Lamoureux, P. Desgroux, F. Liu , Measurements and modeling of laser-induced incandescence of soot at different heights in a flat premixed flame, Appl. Phys. B 118 (2015) 449–469.

[2] Y. Liu, B. Rogg Modelling of Thermally Radiating Diffusion Flames with Detailed Chemistry and Transport, in: Heat Transfer in Radiating and Combusting Systems, Springer, Berlin, Heidelberg, 1991, pp. 114–127.

SM2: Measurement of soot volume fractions and of soot size distributions using HIM microscopy

- **Soot volume fraction profiles measured by LII calibrated by CRDE**

The soot volume fraction f_v was determined from the temporal peak of the measured LII signal $S_{LII}(\lambda)$ according to: $f_v \propto \frac{S_{LII}(\lambda)}{E(m_\lambda).I_{bb}(T,\lambda)}$ where $I_{bb}(T,\lambda)$ is the Planck function, T is the peak soot temperature reached by the particle during the laser heating, λ is the emission wavelength and $E(m_\lambda)$ the soot absorption function .

The temperature of the laser-heated soot particles was obtained by two-color LII by collecting simultaneously the LII emission issued from the collection volume on two photomultipliers tubes (Hamamatsu, R2257) equipped with interference filters centred respectively at 532 with FWHM 8.6 nm and 650 nm with FWHM 10 nm. Measurements were performed using a 1064 nm laser excitation wavelength generated by a Nd:YAG laser (Quantel Brilliant) at 10 Hz with a FWHM pulse duration of 9 ns. The Gaussian laser beam was transformed into a nearly top-hat fluence distribution profile on the burner axis. The collection volume (19 mm^3) was selected in such a way that it expands in the two directions where the soot volume fraction is nearly constant i.e. in the plane parallel to the burner surface (7.2 mm x 5.5 mm), while its vertical axis height is 0.48 mm which is the vertical spatial resolution.

The relative soot volume fraction profiles were obtained by translating the burner vertically. The laser fluence was set at 0.35 J/cm^2 to reach or approach the "plateau" region of the LII fluence curves and to get sufficient LII signal in the very low sooting nucleation flame. LII profiles were corrected for the variation of the temperature of the laser-heated soot particles and of $E(m_\lambda)$ along the HAB as detailed in Betrancourt et al. [3]. The relative variation of $E(m_\lambda)$ with HAB and its spectral dependence as function of the soot maturity was evaluated using a novel approach described in Betrancourt et al [3]. It was found that the smallest soot particles in Flame1.75 have an absorption function 40 % lower than in the burnt gases of Flame1.95. Finally, the calibration of the relative soot volume fraction profiles into absolute value was performed at 10 mm in each flame using CRDE (cavity ring-down extinction) at 1064 nm. The use of this laser wavelength for CRDE and LII prevents any spectral interference with the gas phase.

- **PSDFs measured with HIM**

The collected soot samples were analyzed by a helium-ion microscope (Carl Zeiss Orion Plus) following Hlawacek and Gölzhäuser [4]. The images were recorded at a beam energy of 35 keV and a beam current of 0.4 pA.

The PSDFs obtained by HIM in Betrancourt *et al.* [5] in Flame1.95 at 3.5, 6 and 10 mm and in Flame1.75 at 12 mm represent the geometric diameter of log-normal distribution of the individual primary particles. In all cases, the primary particle diameter was measured using the free software ImageJ (https://imagej.nih.gov/ij/docs/guide/146-30.html#fig:Display-options-Particle-Analyzer, 2016). A similar procedure was used to process the images by Schenk et al. [6]. By studying several samples obtained in the same flame conditions and the same images by different users, the peak of the size distribution is estimated to be affected by ± 0.6 nm in Flame1.95 at 10 mm [5]. The main sources of uncertainty on primary particle diameter obtained by HIM are issued from the sampling procedure. The procedure used a silicon wafer connected to a stepper motor allowing a repetitive swing movement across a horizontal plane parallel to the burner surface [5]. Thus, soot particles are collected thermophoretically and by impaction on the wafer surface. This sampling procedure induces an uncertainty of ± 1 mm on the sampling position (HAB) in the flames. In addition to obtain a good contrast, the number of swings was adjusted regarding the soot concentration. This adjustment is a source of bias for size distributions obtained by HIM. Indeed, the adhesion efficiency of nascent soot particles is less important than for mature soot [7]. This leads to an underestimation of their number relatively to mature soot particles. This occurs especially at 6 and 10 mm in Flame1.95 where both nascent and mature soot are expected to be present [8]. Another source of uncertainties affecting HIM PSDFs is a possible spreading of the particles on the substrate upon impaction giving the appearance of a larger particle [6].

[3] C. Betrancourt, X. Mercier, F. Liu, P. Desgroux, Quantitative measurement of volume fraction profiles of soot of different maturities in premixed flames by extinction-calibrated laser-induced incandescence, Appl. Phys. B 125 (2019) 16.

[4] G. Hlawacek, A. Gölzhäuser, Helium Ion Microscopy, Springer International Publishing, 2016.

[5] C. Betrancourt, F. Liu, P. Desgroux, X. Mercier, A. Faccinetto, M. Salamanca, L. Ruwe, K. Kohse-Höinghaus, D. Emmrich, A. Beyer, A. Gölzhäuser, T. Tritscher , Investigation of the size of the incandescent incipient soot particles in premixed sooting and nucleation flames of *n* -butane using LII, HIM, and 1 nm-SMPS, Aerosol Science and Technology 51 (2017) 1–20.

[6] M. Schenk, S. Lieb, H. Vieker, A. Beyer, A. Gölzhäuser, H. Wang, K. Kohse-Höinghaus , Morphology of nascent soot in ethylene flames, Proceedings of the Combustion Institute 35 (2015) 1879–86.
[7] Z. Li, H. Wang , Thermophoretic force and velocity of nanoparticles in the free molecule regime, Physical Review E 70 (2004).
[8] J. Camacho, S. Lieb, H. Wang , Evolution of size distribution of nascent soot in n- and i-butanol flames, Proceedings of the Combustion Institute 34 (2013) 1853–60.

SM3: Measured and modeled mole fractions profiles

Experimental species mole fraction as function of HAB are provided as txt files:
SM3_DATA_FLAME_1.60.txt
SM3_DATA_FLAME_1.75.txt
SM3_DATA_FLAME_1.95.txt

These raw profiles are not shifted towards the burner. Profiles presented in the manuscript have been shifted to account for the probe perturbation as explained in section 3.1.

Below we present additional species profiles:

a) Sequence of raw experimental species profiles in Flame1.75
b) Mole fraction profiles (experimental and modelled) of C3H4, C4H6, C6H6 and C10H8 in Flame1.60. Experimental profiles are shifted by 1.7 mm towards the burner (see section 3.1)
c) Mole fraction profiles (experimental and modelled) of C3H4, C4H6, C6H6 and C10H8 in Flame1.75. Experimental profiles are shifted by 1.7 mm towards the burner (see section 3.1)
d) Mole fraction profiles (experimental and modelled) of C3H4, C4H6, C6H6 and C10H8 in Flame1.95. Experimental profiles are shifted by 1.7 mm towards the burner (see section 3.1)
e) Probe effect (in addition to Fig. 5): Comparison between the predicted (lines) and the measured (symbols) mole fraction profiles of C_2H_2 in Flame1.75 and Flame1.95. Closed symbols represent the experimental data (open symbols) shifted by 1.7 mm towards the burner surface.

And a discussion in f): Discussion on the important pathways for production of a1, a2 and a4 as predicted by the three mechanisms

a) Illustration of the sequence of species in case of Flame1.75 mentioned in section 2.5
The consumption of ethylene, propene, butene and butadiene (data in supplementary materials SM3) occurs upstream the peak of formation of acetylene, propyne and 1-butyne. Raw profiles, not shifted by 1.7 mm towards the burner.

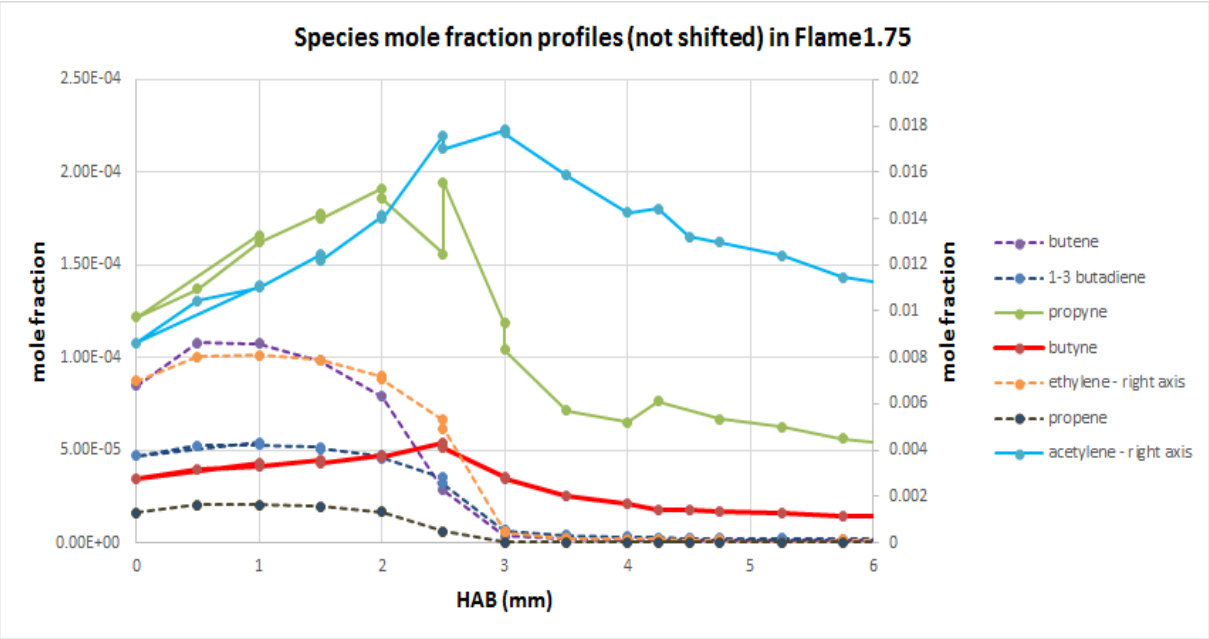

b - Mole fraction profiles (experimental and modelled) of C3H4, C4H6, C6H6 and C10H8 in Flame1.60.
Experimental profiles are shifted by 1.7 mm towards the burner (see section 3.1)

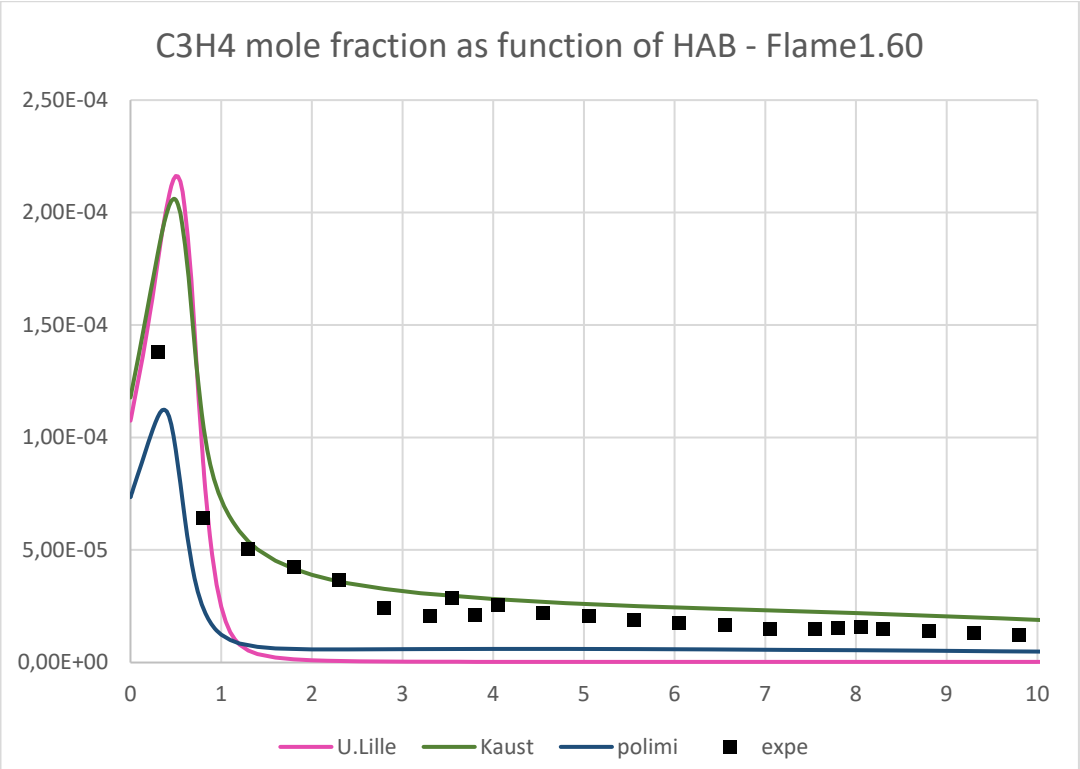

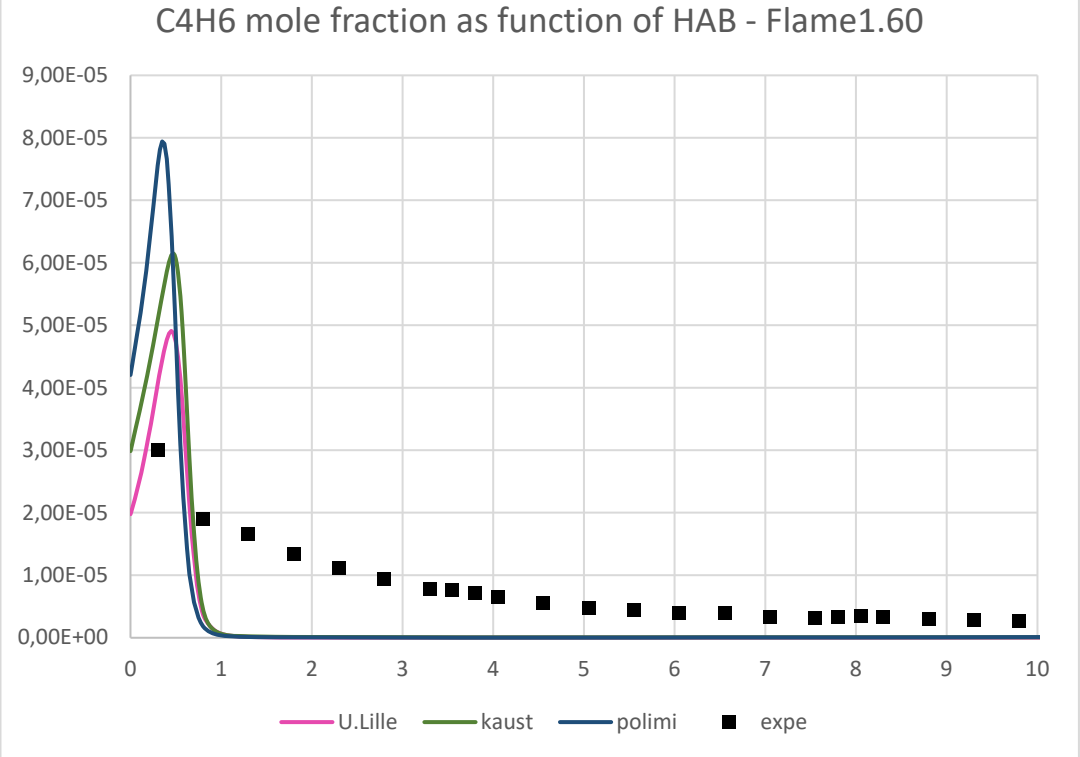

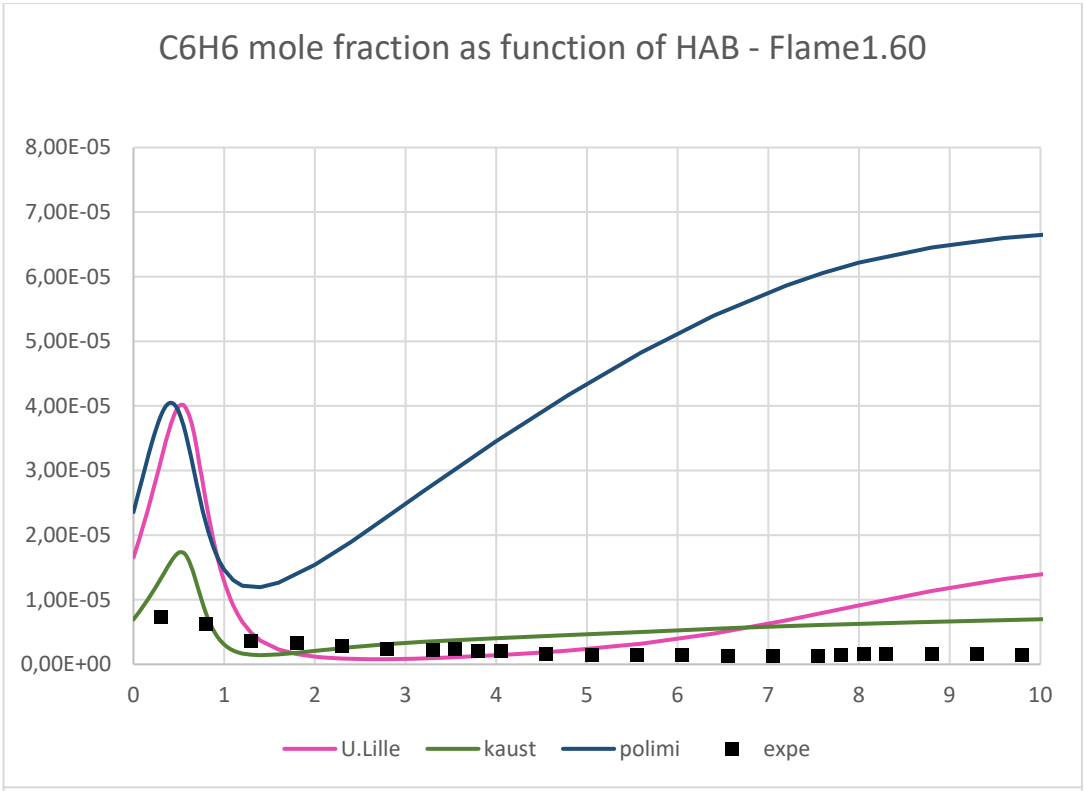
C6H6 mole fraction as function of HAB - Flame1.60
8,00E-05
7,00E-05
6,00E-05
5,00E-05
4,00E-05
3,00E-05
2,00E-05
1,00E-05
0,00E+00
0
1
2
3
4
5
6
7
8
9
10
U.Lille
kaust
polimi
expe

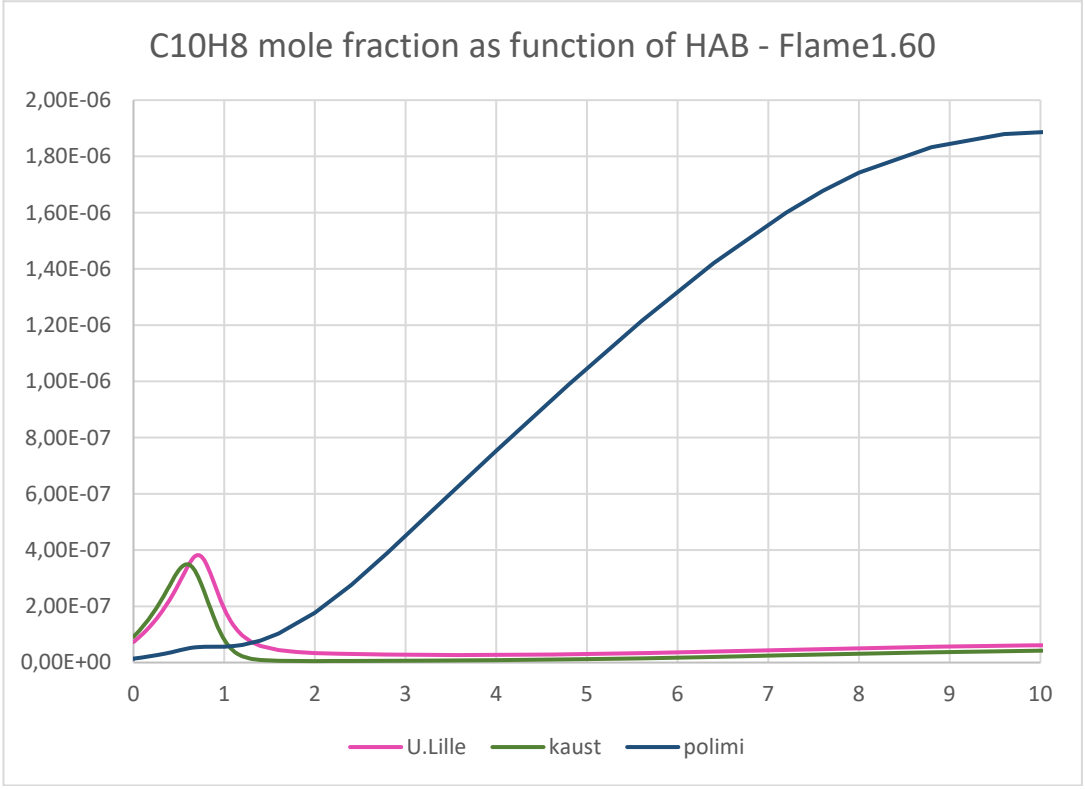
C10H8 mole fraction as function of HAB - Flame1.60
2,00E-06
1,80E-06
1,60E-06
1,40E-06
1,20E-06
1,00E-06
8,00E-07
6,00E-07
4,00E-07
2,00E-07
0,00E+00
0
1
2
3
4
5
6
7
8
9
10
U.Lille
kaust
polimi

c - Mole fraction profiles (experimental and modelled) of C3H4, C4H6, C6H6 and C10H8 in Flame1.75.
Experimental profiles are shifted by 1.7 mm towards the burner (see section 3.1)

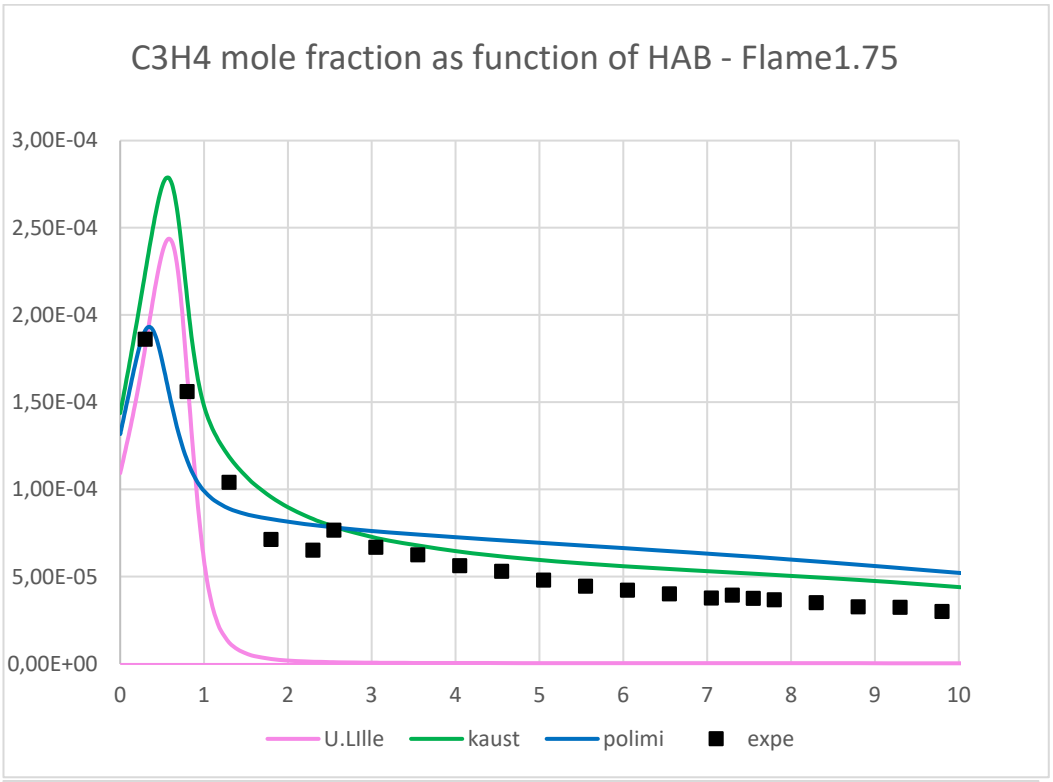

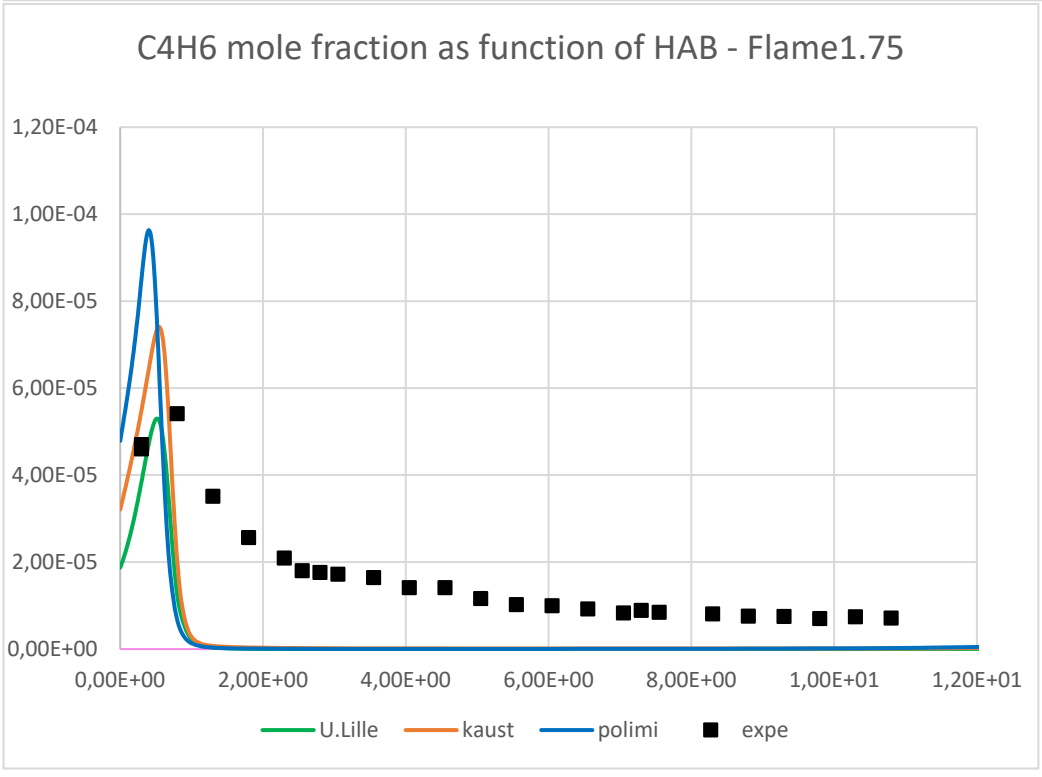

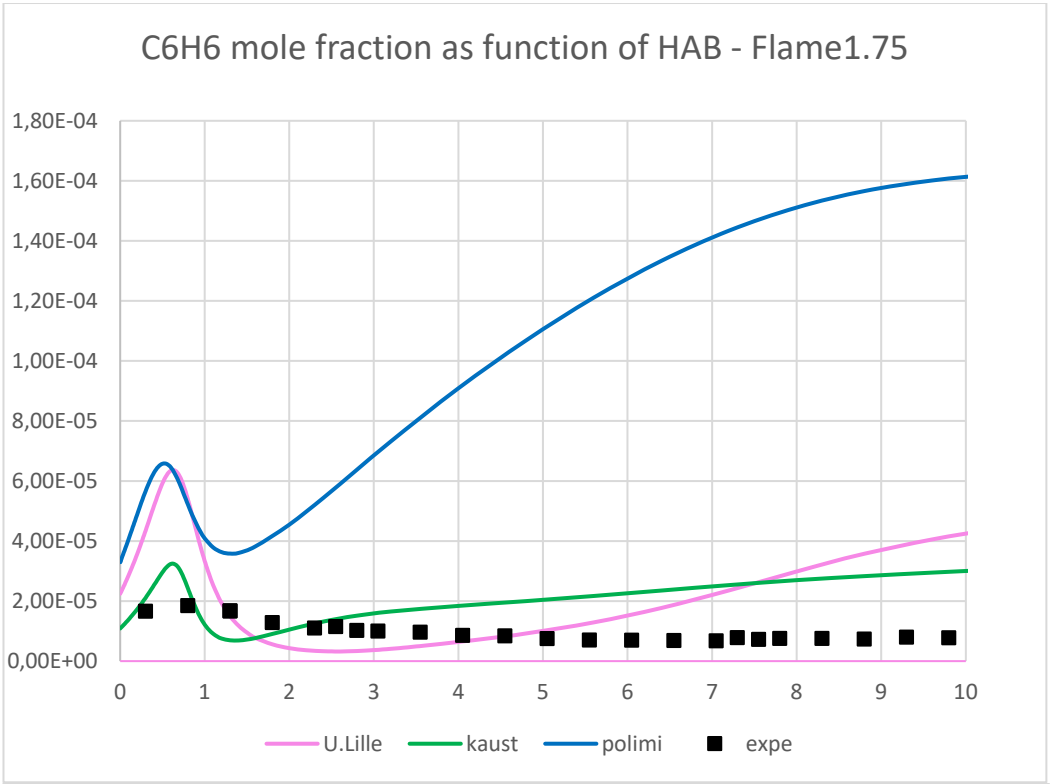
C6H6 mole fraction as function of HAB - Flame1.75
1,80E-04
1,60E-04
1,40E-04
1,20E-04
1,00E-04
8,00E-05
6,00E-05
4,00E-05
2,00E-05
0,00E+00
0
1
2
3
4
5
6
7
8
9
10
U.Lille
kaust
polimi
expe

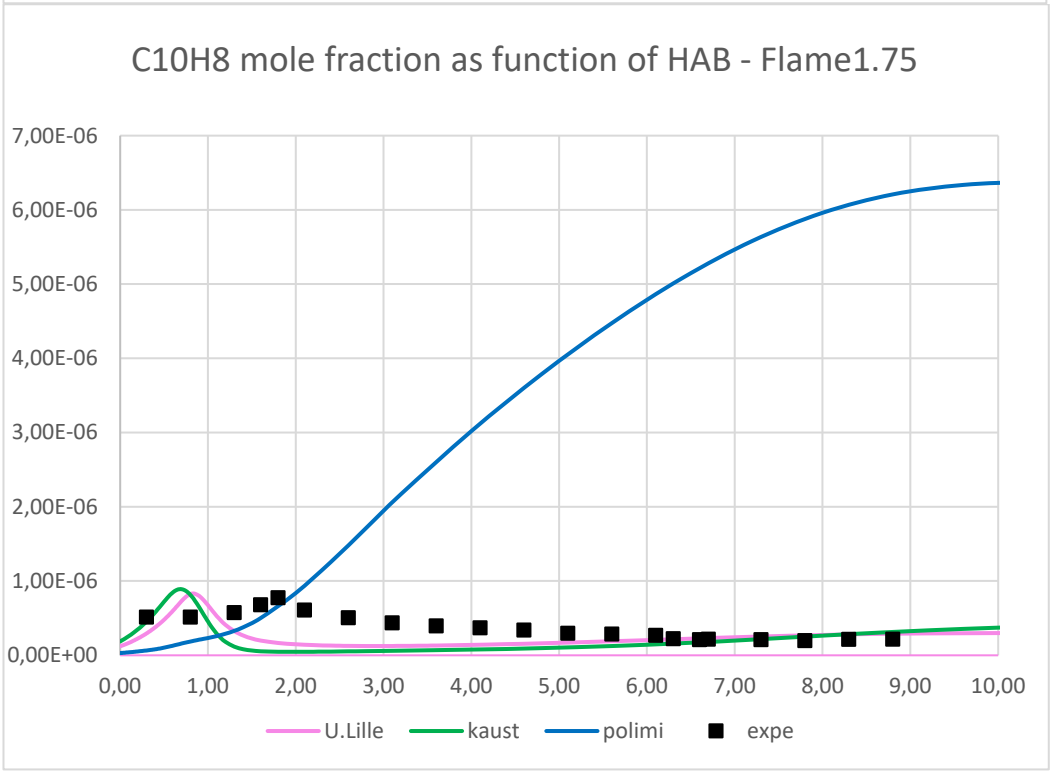
C10H8 mole fraction as function of HAB - Flame1.75
7,00E-06
6,00E-06
5,00E-06
4,00E-06
3,00E-06
2,00E-06
1,00E-06
0,00E+00
0,00
1,00
2,00
3,00
4,00
5,00
6,00
7,00
8,00
9,00
10,00
U.Lille
kaust
polimi
expe

d - Mole fraction profiles (experimental and modelled) of C3H4, C4H6, C6H6 and C10H8 in Flame1.95.
Experimental profiles are shifted by 1.7 mm towards the burner (see section 3.1)

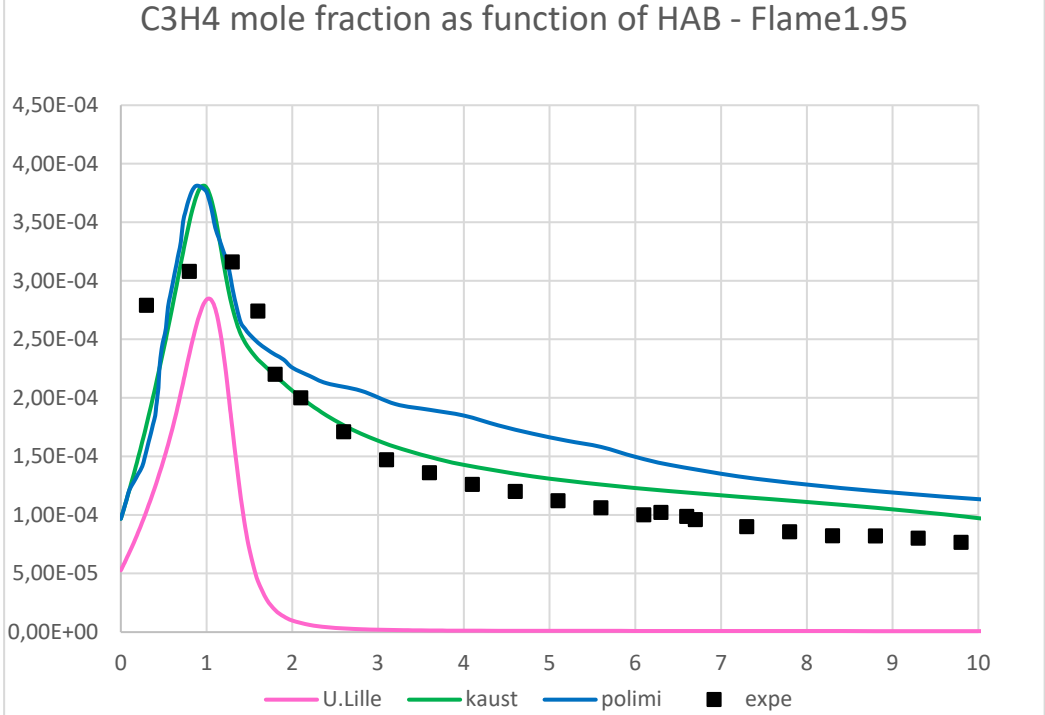

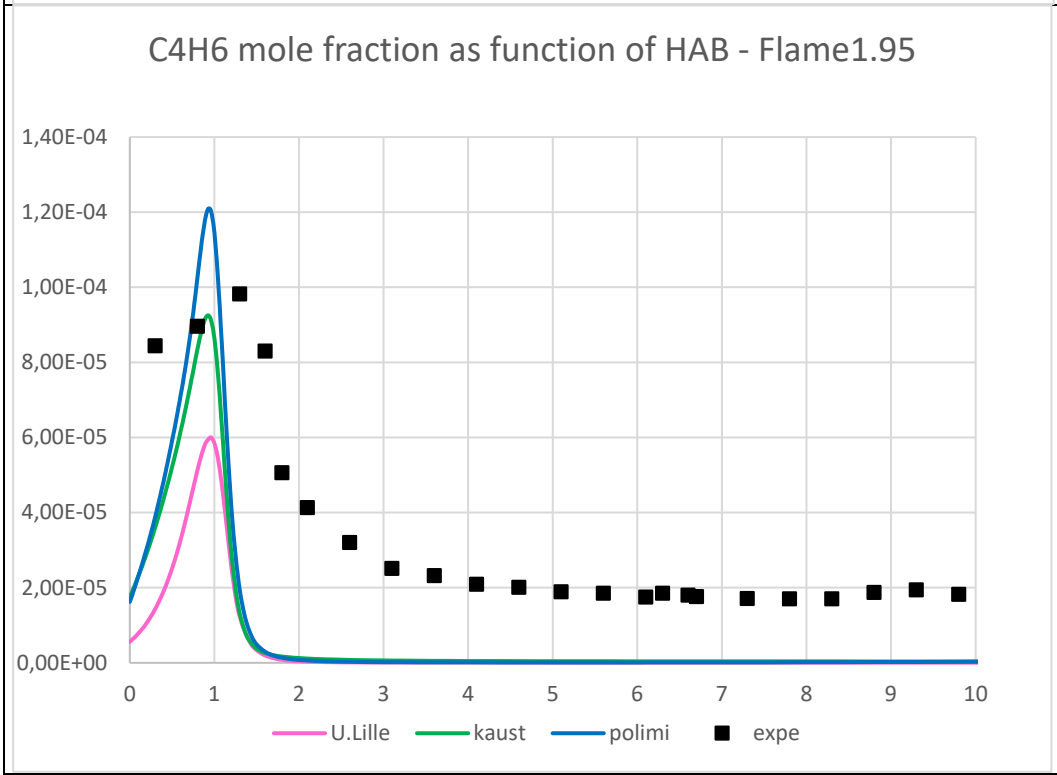

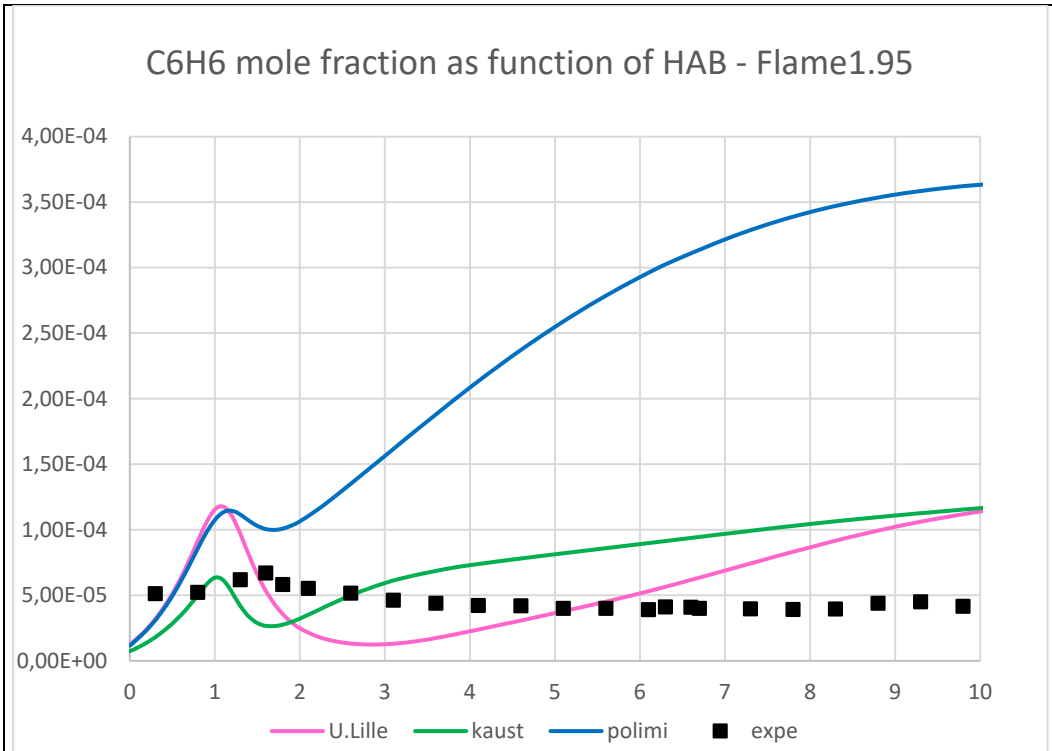
C6H6 mole fraction as function of HAB - Flame1.95
4,00E-04
3,50E-04
3,00E-04
2,50E-04
2,00E-04
1,50E-04
1,00E-04
5,00E-05
0,00E+00
0
1
2
3
4
5
6
7
8
9
10
U.Lille
kaust
polimi
expe

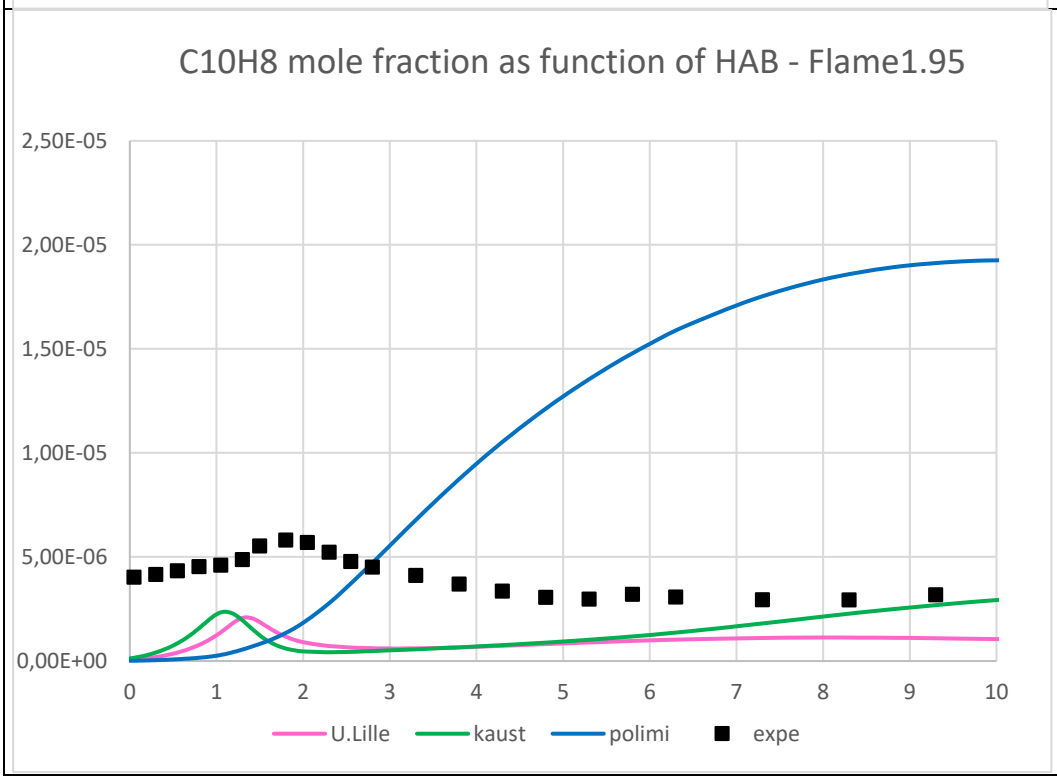
C10H8 mole fraction as function of HAB - Flame1.95
2,50E-05
2,00E-05
1,50E-05
1,00E-05
5,00E-06
0,00E+00
0
1
2
3
4
5
6
7
8
9
10
U.Lille
kaust
polimi
expe

e - Probe effect (in addition to Fig. 5): Comparison between the predicted (lines) and the measured (symbols) mole fraction profiles of C_2H_2 in Flame1.75 and Flame1.95.

Closed symbols represent the experimental data (open symbols) shifted by 1.7 mm towards the burner surface.

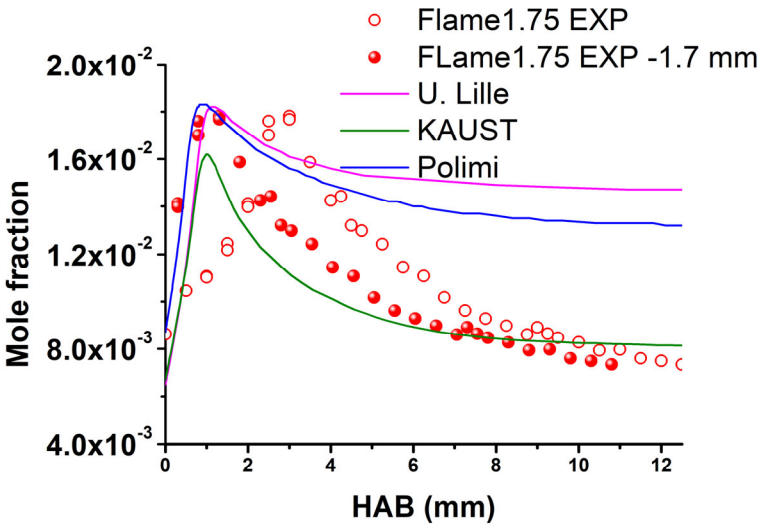

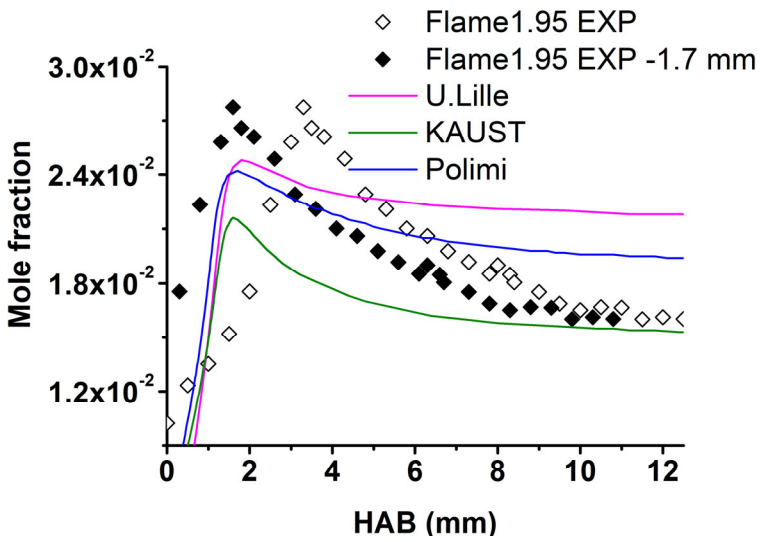

f - Discussion on the important pathways for production of a1, a2 and a4 as predicted by the three mechanisms.

The analysis of the formation pathways of A1, A2 and A4 reveals some differences on the proposed pathways in the three models used in this work. In the following, we point out these differences in the case of the n-butane flame stabilized at equivalence ratio of 1.75. The differences are mainly due to the introduction of different kinetic parameters or the globalization of some processes. This naturally results in different species mole fraction predictions.

A1 formation (benzene):

The three mechanisms agree on the significant contribution to benzene formation via the recombination of phenyl radicals with H atoms (C6H5 + H = A1).

The Ulille and Polimi mechanisms consider the recombination of propargyl radicals (C3H3 + C3H3 = A1) as one of the main sources of the formation of the first aromatic ring while this pathway appears as minor in the KAUST model. The latter is also distinguished by considering a global process leading to the formation of A1 by recombination of propargyl and allyl radicals (C3H3 + AC3H5 = A1 + H + H). In this model, the thermal decomposition of ethylbenzene (A1C2H5 = A1+C2H5) also contributes to benzene formation.

Polimi model includes another global process of benzene formation by reacting methylcycloendiene with hydrogen atoms (MCPTD + H = H + H2 + C6H6). In this model, benzene is also formed from phenol (C6H5OH + H = A1 + H2O). Finally, the Ulille mechanism is the only one to show a main contribution to the formation of benzene by adding acetylene to butadienyl radicals (C2H2 + nC4H5 = A1 + H).

A2 formation (naphtalene):

The three mechanisms agree on a very minor contribution to naphthalene formation by self cyclopendienyl radicals recombination (2C5H5 = A2). The three mechanisms also agree on the contribution to A2 formation by removal of the methyl group from methylnaphthalene by reaction with H atoms (A2CH3 + H = A2 + CH3). Ulille mechanism distinguishes the two possible positions of the methyl group.

On the other hand, the differences appear at the level of the main reactions controlling the formation of A2. In the ULille mechanism, naphthalene is produced mainly by recombination of propargyl and benzyl radicals (C7H7+ C3H3=A2+2H) whereas in the two other models, A2 is recycled by recombination of naphthalenyl radicals A2* with H atoms (A2* +H = A2) or by reaction with H2O (A2*+H2O = A2 + OH). It should be noted that Polimi mechanism does not distinguish between A2* radicals.

A4 formation (pyrene):

In the three mechanisms, pyrene is recycled by recombination of pyrenyl (A4*) radicals with H atoms (A4*+H=A4). On the other hand, the polimi model is the only one that does not distinguish the possible radical sites. It is also the only one to significantly produce pyrene by oxidation of a BIN structure by OH radicals (BIN1B+OH = 0.75BIN1B+0.25A4+HCO). This reaction governs A4 formation and largely counterbalances the main reaction of consumption of pyrene by H-abstraction by hydrogen atoms (A4+H=H2+A*). The contribution of the C-addition mechanism to the formation of A4 from A3 by addition of C2H2 on A*3 radicals (A3* + C2H2= A4 + H) appears not negligible in Ulille and Kaust mechanisms. This contribution is totally absent in the case of Polimi model. On the other hand, the addition of acetylene on A4* radicals (supposed to consume pyrene) leads to the formation of a BIN structure and pyrene (A4*+ C2H2= 0.50BIN1B+0.50A4+H). These elements are most likely the cause of excessive accumulation of pyrene in the post flame region compared to the two other models.

SM4: Soot diameter profiles

Figure 2 shows the mean diameter d_{2nm} of soot predicted by the model i.e. the arithmetic mean diameter computed only with particles larger than 2nm, compared to the primary particle diameter determined by HIM in Flame1.95 and by 1nm-SMPS and HIM in Flame1.75 (section 2.5). The modeled diameters are shown with a cut-off size of 2nm for two reasons. Unlike the previous simulation works involving "nucleation flames" [9] α_{HACA} has not been adjusted to reproduce the very low size growth of soot particles in Flame1.75.

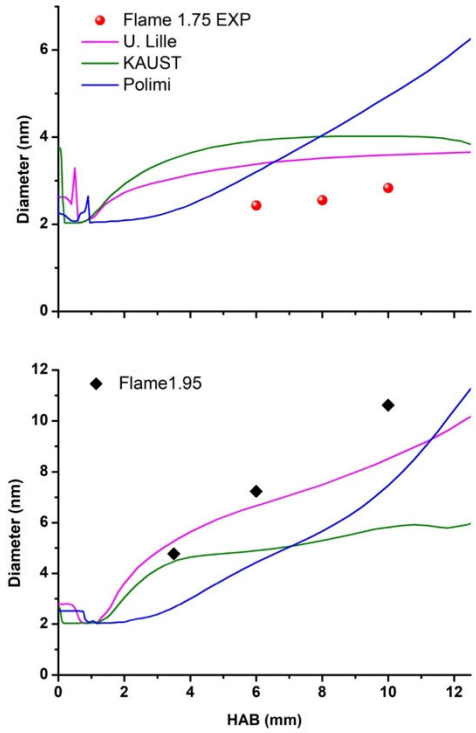

Figure 2: Flame1.75 (top) and Flame1.95 (bottom): measured (symbols) and modeled (lines) soot mean diameter profiles, using U.Lille (pink), Kaust (green) and Polimi(blue) mechanisms. The experimental diameter is primary particle diameter measured by 1nm-SMPS (Flame1.75) and HIM (Flame1.95) whereas the numerical diameter is the mean diameter with a 2nm size cut-off d_{2nm}

For both flames, using either U.Lille or Kaust mechanism, the shift observed on SVF is also observed on diameters and is discussed in section 3.2.2. However, the predicted mean diameters values are remarkably consistent with the measured ones for Flame1.75. They are overestimated of 1 to 1.5nm but they are constant with respect to HAB as observed experimentally. Flame1.95 simulations results agreement with the experimental observations is also very good using U.Lille mechanism while the diameters are underpredicted after 4mm HAB using Kaust mechanism. This difference is mainly due to the difference in pyrene profile, Kaust predicting between 2 and 3 times more pyrene than U.Lille in the burned gases region. All simulations performed using the Polimi mechanism predict diameters notably differently than the ones using the two other mechanisms. This is attributed to the overproduction of small particles because of the much higher pyrene concentrations predicted by this mechanism and also to the value of α_{HACA} that had to be used to minimize the SVF (still overpredicted) which prevents soot growth in size from acetylene addition.

[9] D. Aubagnac-Karkar, A. El Bakali, P. Desgroux, Soot particles inception and PAH condensation modelling applied in a soot model utilizing a sectional method, Combust. Flame 189 (2018) 190–206